Open access • Journal Article • DOI:10.1021/NN5047585

Sulfur-graphene nanostructured cathodes via ball-milling for high-performance lithium-sulfur batteries. — Source link

Jiantie Xu, Jianglan Shui, Jianli Wang, Jianli Wang ...+7 more authors

Institutions: University of Wollongong, Case Western Reserve University, Bragg Institute, Ulsan National Institute of Science and Technology

Published on: 13 Oct 2014 - ACS Nano (American Chemical Society)

1-1-2014

Sulfur-graphene nanostructured cathodes via ball-milling for high-performance lithium-sulfur batteries

Jiantie Xu
University of Wollongong, jx307@uowmail.edu.au

Jianglan Shui
Case Western Reserve University

Jianli Wang
University of Wollongong, jianli@uow.edu.au

Min Wang
Case Western Reserve University

Hua-Kun Liu
University of Wollongong, hua@uow.edu.au

See next page for additional authors

Sulfur-graphene nanostructured cathodes via ball-milling for high-performance lithium-sulfur batteries

Abstract

Although much progress has been made to develop high-performance lithium-sulfur batteries (LSBs), the reported physical or chemical routes to sulfur cathode materials are often multistep/complex and even involve environmentally hazardous reagents, and hence are infeasible for mass production. Here, we report a simple ball-milling technique to combine both the physical and chemical routes into a one-step process for low-cost, scalable, and eco-friendly production of graphene nanoplatelets (GnPs) edge-functionalized with sulfur (S-GnPs) as highly efficient LSB cathode materials of practical significance. LSBs based on the S-GnP cathode materials, produced by ball-milling 70 wt % sulfur and 30 wt % graphite, delivered a high initial reversible capacity of 1265.3 mAh g-1 at 0.1 C in the voltage range of 1.5-3.0 V with an excellent rate capability, followed by a high reversible capacity of 966.1 mAh g-1 at 2 C with a low capacity decay rate of 0.099% per cycle over 500 cycles, outperformed the current state-of-the-art cathode materials for LSBs. The observed excellent electrochemical performance can be attributed to a 3D "sandwich-like" structure of S-GnPs with an enhanced ionic conductivity and lithium insertion/extraction capacity during the discharge-charge process. Furthermore, a low-cost porous carbon paper pyrolyzed from common filter paper was inserted between the 0.7S-0.3GnP electrode and porous polypropylene film separator to reduce/eliminate the dissolution of physically adsorbed polysulfide into the electrolyte and subsequent cross-deposition on the anode, leading to further improved capacity and cycling stability.

Keywords

lithium, batteries, high, performance, milling, sulfur, ball, via, cathodes, nanostructured, graphene

Disciplines

Engineering | Physical Sciences and Mathematics

Publication Details

Xu, J., Shui, J., Wang, J., Wang, M., Liu, H., Dou, S. Xue., Jeon, I., Seo, J., Baek, J. & Dai, L. (2014). Sulfur-graphene nanostructured cathodes via ball-milling for high-performance lithium-sulfur batteries. ACS Nano, 8 (10), 10920-10930.

Authors

Jiantie Xu, Jianglan Shui, Jianli Wang, Min Wang, Hua-Kun Liu, S X. Dou, In-Yup Jeon, Jeong-Min Seo, Jong-Beom Baek, and Liming Dai

Sulfur-Graphene Nanostructured Cathodes via Ball-Milling for High-Performance Lithium-Sulfur Batteries

Jiantie Xu[a,b], Jianglan Shui[b], Jianli Wang[a,c], Min Wang[b], Huakun Liu[a], Shixue Dou[a,] In-Yup Jeon[d], Jeong-Min Seo[d], Jong-Beom Baek[d,*], and Liming Dai[b,*]*

[a]*Institute for Superconducting and Electronic Materials, University of Wollongong, Wollongong, NSW 2522, Australia*

[b]*Department of Macromolecular Science and Engineering, School of Engineering, Case Western Reserve University, Cleveland, OH 44106, United States of America*

[c]*Bragg Institute, Australian Nuclear Science and Technology Organization, Lucas Heights, NSW 2234, Australia*

[d]*School of Energy and Chemical Engineering/Low-Dimensional Carbon Materials Center, Ulsan National Institute of Science and Technology (UNIST), Banyeon, Ulsan 689-798, South Korea*

Correspondence author E-mails: liming.dai@case.edu; jbbaek@unist.ac.kr; shi_dou@uow.edu.au

Abstract

Sulfur has recently received considerable attention as the cathode material for lithium-sulfur batteries (LSBs) because of its higher theoretical capacity (~ 1675 mAh g^{-1}) and energy density (~ 2600 Wh kg^{-1}). Although much progress has been made to develop high-performance LSBs, the reported physical or chemical routes to sulfur cathode materials are often multistep/complex and even with environmentally hazardous reagents, and hence infeasible for mass production. Here, we report a simple ball-milling technique to combine both the physical and chemical routes into one-step process for low-cost, scalable, and eco-friendly production of graphene nanoplatelets (GnPs) edge-functionalized with sulfur (S-GnPs) as highly-efficient LSB cathode materials of practical significance. LSBs based on the S-GnPs cathode produced by ball-milling 70 wt% sulfur and 30 wt% graphite delivered a high initial reversible capacity of 1265.3 mAh g^{-1} at 0.1 C in the voltage range of 1.5 - 3.0 V

with an excellent rate capability, followed by a high reversible capacity of 966.1 mAh g^{-1} at 2 C with a low capacity decay rate of 0.099% per cycle over 500 cycles - outperformed the current state-of-the-art cathode materials for LSBs. The observed excellent electrochemical performance is attributable to the 3D porous 'sandwich-like' structure of S-GnPs, coupled with the newly-discovered 'spin-effect' induced by S-doping, leading to enhanced ionic conductivity and lithium insertion/extraction during the discharge-charge process.

With the global energy consumption, along with air pollution and associated global warming, accelerating at an alarming rate, it has become more important than ever to develop electric vehicles (EVs) with low greenhouse gas emissions (GHG, such as CO_2 and CH_4). However, the large-scale application of EVs for transportation will not be realized if there is no cost-effective commercialization capability for the development of electrical energy storage systems of high specific energy, high power density, and long cycle life. So far, lithium ion batteries (LIBs) have been widely used as the state-of-the-art energy storage system in various portable and smart devices, including cell phones, MP3 devices, cameras, and laptops, due to their high energy density and long cycle life[1, 2]. Nevertheless, the specific capacities that can be obtained from current cathode materials for LIBs are insufficient to meet the ever increasing requirements for EV and other energy-demanding applications. In comparison with current state-of-the-art cathode materials, such as lithium metal oxides (140 ─ 200 mAh g^{-1} and 500 ─ 700 Wh kg^{-1}) and lithium metal phosphates (140 ─ 190 mAh g^{-1} and 560 ─ 800 Wh kg^{-1}), sulfur has recently received considerable attention as the cathode material for lithium-sulfur batteries (LSBs) because of its much higher theoretical capacity (~ 1675 mAh g^{-1}) and energy density (~ 2600 Wh kg^{-1})[3]. This, together with its low cost, earth abundance, and eco-friendliness, makes sulfur as one of the most promising cathode materials for next generation LIBs. However, sulfur-based cathode materials are still suffered from multiple drawbacks, including 1) the low electrical conductivity of sulfur S_8 (5×10^{-30} S cm^{-1} at 25 ^{o}C); 2) the large volume (~ 76%) and morphology changes of the sulfur electrodes during the discharge-charge process; and 3) the easiness with which intermediate products (*e.g.*, lithium polysulphides, $Li_2S_{4\text{-}8}$, Li_2S_2, Li_2S) can be dissolved ($Li_2S_{4\text{-}8}$) in the electrolyte solution or deposited (Li_2S_2, Li_2S) on the lithium anode surface to increase the resistance and shorten the cycle life[4, 5].

To overcome the above-mentioned obstacles, carbon based materials with various hierarchical structures, including meso-/micro-porous carbons[6-11], hollow carbon spheres[12-14], carbon nanotubes/nanofibers[15-19], graphene derivatives[20-30], and flexible carbon membranes[31], have been developed as conductive and structurally stable supports for compositing with sulfur. Meanwhile, coating the sulfur cathodes with appropriate polymers (*e.g.*, conducting polymers) was demonstrated to not only effectively eliminate the dissolution of sulfur into the electrolyte solution but also reduce volume expansion of the sulfur electrode, leading to enhanced cycling stability[32-37]. On the other hand, both physical and chemical routes have been devised for the preparation of LSB cathode materials from sulfur composites with carbon materials or polymers. Examples include LSB cathodes based on sulfur mixed with either meso-porous single-walled carbon nanotube (SWCNT)-graphene[18] or three-dimensional (3D) 'sandwich-like' cetyltrimethylammonium bromide (CTAB)─graphene oxide (GO) hybrids (up to 800 mAh g^{-1} at 6 C with a low decay rate of 0.039% per cycle over 1500 cycles)[25], a sulfur-graphene composite with ~ 63.6 wt% sulfur uniformly coated on graphene through reduction of GO and concomitant sulfurization (440 mAh g^{-1} after 500 cycles at 0.75 C)[22], and polyvinylpyrrolidone (PVP)-encapsulated hollow S nanospheres (*i.e.*, S@PVP nanospheres) from the reaction of $Na_2S_2O_3$ and HCl in an aqueous of PVP (849 mAh g^{-1} at 2 C with a capacity decay of 0.046% per cycle over 1000 cycles at 0.5 C)[35]. Although much progress has been made, the achieved capacities for sulfur-composite cathodes are still far below than the theoretical value (*i.e.*, ~ 1675 mAh g^{-1}). Furthermore, most of the reported physical and chemical routes to sulfur composites are multistep and complex, and hence too expensive for mass production; they often involve environmentally hazardous reagents (*e.g.*, strong acids for GO production by Hummers' method)[38].

We have recently developed a simple low-cost, but effective and eco-friendly, ball-milling method for large-scale production of various graphene nanoplatelets (GnPs) edge-functionalized with different moieties without the basal plane damage, and hence good electrical/thermal conductivity[39-42]. Through the one-step ball-milling of graphite in the presence of sulfur (Fig. S1, Supporting Information), we revealed in the present study that sulfur can not only act as a chemical reagent to produce GnPs edge-functionalized with sulfur (S-GnPs) but also homogenously adsorbed on and intercalated into the GnPs, leading to highly efficient LSB cathode materials. Thus, the ball-milling technique effectively combines both the physical and chemical routes into one-step process for low-cost, scalable, and eco-friendly production of highly-efficient LSB

cathode materials of practical significance. We found that LSBs based on the S-GnPs cathode produced by ball-milling 70 wt% sulfur and 30 wt% graphite (denoted as: 0.7S-0.3GnP) delivered a high initial reversible capacity of 1265.3 mAh g^{-1} at 0.1 C in the voltage range of 1.5 - 3.0 V with an excellent rate capability, followed by a high reversible capacity of 966.1 mAh g^{-1} at 2 C with a low capacity decay rate of 0.099% per cycle over 500 cycles. Both the initial and reversible capacities observed for the 0.7S-0.3GnP are among the highest values reported so far,[11, 25, 28, 37] attributable to its 3D porous 'sandwich-like' structure (*vide infra*), coupled with the newly-discovered 'spin-effect' induced by S-doping, leading to enhanced ionic conductivity and lithium insertion/extraction during the discharge-charge process.

Material preparation, morphology and structural analysis. Fig. 1a shows the schematic representation of the S-GnP preparation. Briefly, stoichiometric amounts of commercial graphite and sulfur were placed into a stainless steel jar containing stainless steel balls and sealed under argon for agitating at 500 rpm for 48 h in a planetary ball-mill machine (TCI, USA). The resultant *x*S-*y*GnP (*x* and *y* represent the weight percentage of S and graphite, respectively, in the starting material) powder was then heated at 700 °C with a temperature ramp of 2 ^{o}C min^{-1} in a tube furnace for 2 h under an argon flow (1000 s.c.c.m.) to remove physically adsorbed sulfur from the final product (designated as: *x*S-*y*GnP-700°C). Fig. 1b-e reproduces scanning electron microscope (SEM) images of the S-GnP samples with different sulfur loadings from 50 to 80 wt%, which show large particles of ~ 3-10 μm in size with a similar morphology to that of sulfur (Fig. S1b) but different from the 'plate-like' graphite (Fig. S1a). More close examination under a higher magnification (Fig. 1f-i) revealed a morphological change from the "sulfur-like" bulk particles (Fig. 1f, 0.5S-0.5GnP), through randomly-distributed fragments with meso-/macro-pores (Fig. 1g, 0.6S-0.4GnP) and "sandwich-like" layered meso-/macro-pores (Fig. 1h, 0.7S-0.3GnP), to a uniform meso-/macro-porous structure (Fig. 1i, 0.8S-0.2GnP), indicating that the presence of sulfur in the ball-milled graphite facilitated the formation of 3D nanostructured carbon foams, presumably due to the strong S-S interaction between the edge-functionalized S-GnP particles. While the edge-functionalization without basal plane damage would ensure good electrical/thermal conductivities for the resultant 3D network, the meso-/macro-porous structures in both the 'sandwich-like' and "foam-like' S-GnPs with a relatively large specific surface area (138.1 ~ 182.6 m^2 g^{-1}, Table S1) could allow for an efficient sulfur dispersion between the

mechanically-stable GnP networks to alleviate the volume expansion/shrinkage of sulfur even during repeated discharge-charge cycles.

Fig. 1j shows a typical TEM image for 0.7S-0.3GnP with the corresponding selected area electron diffraction (SAED) patterns at the edge (top inset) and basal plane (bottom inset), respectively. Compared to the bottom SAED pattern in the inset of Fig. 1j, the more diffusive rings shown in the top SAED pattern indicates a more amorphous carbon edge, as also revealed by the edge-on view of TEM image given in Fig. 1j. While the edge-functionalization of GnPs by ball milling in general has been verified in our previous studies[39-42], we further carried out the energy dispersive spectroscopic (EDS) mapping for 0.7S-0.3GnP. As shown in Fig. 1k-m, sulfur, carbon and oxygen all uniformly distributed throughout the sample. The observed homogenous distribution of sulfur for the S-edge-functionalized GnP could be taken as an evidence for the homogenous adsorption/intercalation of sulfur on/into the GnPs, as mentioned above, though it can also be rationalized by considering the fact that the EDS sample consists of randomly overlapped multilayer GnPs. The presence of oxygen is due to the post-ball-milling conversion of the reactive edge-sulfur and carbon species into oxygen-containing functional groups, such as -OH, -SO_2, -COOH, and -SO_3H through spontaneous reactions with oxygen/moisture in air upon opening the ball-milling reactor[42].

To further investigate chemical structures of the S-GnP samples, we performed X-ray photoelectron spectroscopic (XPS) measurements. As expected, XPS survey spectra for all of the S-GnPs showed O 1s, C 1s, S 2s, and S 2p peaks at ~ 534 eV, ~ 285 eV, ~ 229 eV, and ~ 165 eV, respectively (Fig. 2a)[42]. The high-resolution XPS O 1s, C 1s and S 2p spectra of the 0.7S-0.3GnP sample were shown in Fig. S2a-c, respectively. As can be seen in Fig. S2a, the C1s peak can be deconvoluted into three peaks attributable to C-C bond at 285.1 eV, C-OH and C-S at 286.1 eV, and O=C-OH at 289.6 eV while the corresponding O1s spectrum shows O=C-OH and C-OH peaks at 532.2 and 533.9 eV, respectively (Fig. S2b). The S2p peak was well fitted to C-SO_3 at 168.3 eV and C-S at 165.2 /164.3 eV[42].

Thermogravimetric analyses (TGA) were performed under argon atmosphere to estimate the sulfur content in the S-GnP samples. Fig. 2b shows significant weight losses over 200 ─ 500 °C for all of the S-GnP samples, due, most probably, to the evaporation of physically adsorbed sulfur. At 700 °C, the non-stoichiometric weight losses for the S-GnP samples were 44.4% (0.5S-0.5GnP), 55.6% (0.6S-0.4GnP), 65.5% (0.7S-0.3GnP), and 75.8% (0.8S-0.2GnP), indicating that

about 4 wt% (Table S2) sulfur has been chemically doped in the carbon networks. To confirm the chemical doping with sulfur, we heated up the 0.7S-0.3GnP at 700 °C under argon for 2 hours, and then purified by washing with 1M HCl (the final product was designed as: 0.7S-0.3GnP-700°C -1M HCl) to remove physically adsorbed S and Fe residues from the ball-milling reactor and steel ball, if any. As shown in Fig. S3, the XRD pattern of 0.7S-0.3GnP before the heating/HCl washing revealed characteristic peaks for the crystalline sulfur, indicating a complete exfoliation for the GnP (*cf.* Fig. 2e). Upon heating up to 700 °C with and without the HCl washing, all the sulfur peaks disappeared whereas the typical graphitic carbon peak (*cf.* Fig. 2e) appeared (Fig. S3), indicating that the exfoliated GnP partially restacked during the heat treatment due to the removal of the absorbed sulfur. However, the presence of the XPS peaks of sulfur in Fig. 2c and S2f and the corresponding elemental EDS mapping (Fig. S4b) for 0.7S-0.3GnP-700°C -1M HCl clearly indicate that a considerable amount (3.8 at%, Table S2) of S-dopants have been strongly bonded into the carbon network through C-S (164.5 eV and 165.9 eV) and C-SO_3 (168.3 eV) bonds, apart from those physically adsorbed sulfur.

Fig. 2d shows typical Raman spectra for the pristine graphite, sulfur, and S-GnPs. A comparison of spectra for the S-GnPs to that of sulfur in Fig. 2d indicates the sulfur origin for those peaks in the range of 50 - 525 cm^{-1}. In addition, the S-GnP samples exhibited two peaks at ~ 1330 and ~ 1600 cm^{-1} characteristic of the D and G bands, respectively[39-42]. For all the S-GnPs, the intensity of the D band is higher than that of the G band due to the presence of defects induced by S-doping. Fig. 2d further shows that the relative peak intensities of the sulfur peaks to the GnP peaks increased with increasing mass ratio of S/GnP. As shown in Fig. 2d and Fig. S5, the G band for all of the S-GnP samples can be fitted into two sub-peaks (A and B in Fig. S5), indicating the successful doping of S heteroatoms into the carbon networks, as is the case for N-doped graphene sheets.[43]

Fig. 2e shows X-ray diffraction (XRD) patterns of the pristine graphite, sulfur, and S-GnPs. As expected, the pristine graphite exhibited a prominent (002) peak at 26.5°, corresponding to an interlayer *d*-spacing of 0.34 nm, as well as two characterized peaks ((101) peak at 44.8° and (004) peak at 54.8°)[44]. The salient feature to note is that the ball-milling caused a high degree of exfoliation, as reflected by the dramatic reduction in intensity for graphitic peaks, along with a concomitant down-shift of the (002) band with increasing sulfur content, in a good consistence with the Raman results (Fig. 2d). The almost fully exfoliated S-GnPs with a large surface area,

good electrical conductivity, and meso-/micro-pores are ideal LSB cathode materials, as described below.

Electrochemical performance. Fig. 3a shows typical discharge-charge profiles for the S-GnP cathodes at 0.1C over 1.5 - 3.0 V. During the discharge process, two plateaus at ~ 2.35 V and ~ 2.10 V were seen for all of the S-GnP samples, corresponding to the intercalation of lithium into S_8 to form a long chain (Li_2Sx, $2 \leq x \leq 4$) and short chain (Li_2Sx, $1 \leq x \leq 2$) of lithium polysulfides, respectively. The discharge-charge profiles for 0.7S-0.3GnP at various C-rates are given in Fig. 3b, which shows increasingly shortened discharge-charge plateaus with increasing C-rate due to electrode polarization. Similar electrochemical behavior has been previously reported for sulfur cathodes in LIBs[7, 8]. To test the rate and cycling performance, we discharged and charged LSBs based on the S-GnP cathodes for 90 cycles in the voltage range of 1.5 - 3.0 V at C-rates from 0.1 C to 10 C (Fig. 3c). As can be seen, the 0.6S-0.4GnP cathode showed the highest initial discharge capacity of 1356.3 mAh g^{-1} at 0.1 C, followed by the 0.5S-0.5GnP (1311.7 mAh g^{-1}), and then the 0.7S-0.3GnP (1265.3 mAh g^{-1}) and 0.8S-0.2GnP (889.5 mAh g^{-1}), and all are among the highest values reported so far[11, 25, 28, 37]. By increasing the C rate from 0.2 to 10 C, however, the 0.7S-0.3GnP cathode showed the highest reversible capacity and rate capability (inset of Fig. 3c) among all the S-GnPs studied in this work. The average discharge capacities of the 0.7S-0.3GnP cathode at 0.2 C, 0.5 C, 1 C, 2 C, 5 C and 10 C were 1043.1, 885.6, 756.8, 610.4, 404.8, and 186.5 mAh g^{-1}, respectively. When the C-rate was reduced back to 0.1 C after 80 cycles, the 0.7S-0.3GnP cathode can still deliver a higher reversible discharge capacity of 1063.2 mAh g^{-1} than those of 0.5S-0.5GnP (762.4 mAh g^{-1}), 0.6S-0.4GnP (817.8 mAh g^{-1}), and 0.8S-0.2GnP (598.1 mAh g^{-1}) as well as many reported LSB cathodes LIBs[11, 25, 28, 37].

The excellent electrochemical stability of 0.7S-0.3GnP was also supported by cyclic voltammetry (CV) curves in Fig. S6a, which shows highly overlapping CV curves over 4 cycles at 0.1 mV s^{-1} with well-defined and strong redox peaks even after 90 cycles (Fig. S6a). To investigate the kinetics of the S-GnP cathodes, we compared the electrochemical impedance spectroscopic (EIS) results for the cells cycled over 90 cycles. As shown in Fig. S6b, the impedance curves for all of the S-GnP samples exhibited two apparent semicircles in the high and medium frequency regions, attributable to the lithium ion diffusion through the electrolyte (R_e) (intercept of the 1st semicircle), the solid electrolyte interface (SEI) film resistance (R_s) (diameter

of the 1st semicircle), and the charge transfer resistance (R_{ct}) (diameter of the 2nd semicircle). The ~ 45° inclined line in the low-frequency range corresponds to a Warburg impedance[45]. The equivalent circuit model (inset of Fig. S6b) was constructed to analyze the impedance spectra. The fitting results from this model are listed in Table S3. The lowest R_{ct} (79.9 Ω) and R_s (34.5 Ω) seen in Table S3 indicate the highest ionic conductivity for 0.7S-0.3GnP among all of the S-GnP samples investigated in the present study.

The S-GnP cathodes were further subjected to testing the relatively long cycling performance at 2 C in the voltage range of 1.5 - 3.0 V. Fig. 3d shows initial discharge capacities of 966.1 mAh g^{-1} (0.7S-0.3GnP), 919.9 mAh g^{-1} (0.6S-0.4GnP), 722.7 mAh g^{-1} (0.5S-0.5GnP), and 483.2 mAh g^{-1} (0.8S-0.2GnP). After 500 cycles, these S-GnP cells can maintain discharge capacities of 485.6 mAh g^{-1} (0.7S-0.3GnP), 352.9 mAh g^{-1} (0.5S-0.5GnP), 344.8 mAh g^{-1} (0.6S-0.4GnP), and 200.2 mAh g^{-1} (0.8S-0.2GnP) with the initial capacity retentions of 50.3%, 48.8%, 37.5%, and 41.4%, corresponding to the capacity decay rate of 0.099%, 0.102%, 0.125%, and 0.117% per cycle, respectively. Despite their differences in the capacity and capacity retention, all of the S-GnP electrodes showed high Coulombic efficiencies around 100% due to their excellent structural stability during each of the discharge-charge cycles. Among all of the S-GnP cathodes, the 0.7S-0.3GnP showed the highest capacity and capacity retention at 2 C over 500 cycles due, most probably, to its unique 3D porous 'sandwich-like' structure (*cf.* Fig. 1h) with a large surface area, good electronic/ionic conductivity, and high sulfur uptake. In addition, we found that the magnetic effect induced by S-doping[41, 42] also makes its contribution to the excellent cathodic performance of the S-GnP samples

Spin effect of S-GnP. We measured magnetic properties for the 0.7S-0.3GnP and found ferromagnetic behavior with a hysteresis loop under 0.4 T magnetic field at 300 K (Fig. 4b) and 5 K (Fig. 4c), though 0.7S-0.3GnP exhibited apparent diamagnetic behavior with a magnetic susceptibility (χ) of -1.88×10^{-6} above 0.4 T (Fig. 4a). To rule out possible effects of any Fe impurities from the ball-milling reactor and steel balls during ball-milling, we further measured the magnetic properties of 0.7S-0.3GnP-700ºC-1M HCl for comparison. Unlike 0.7S-0.3GnP, the 0.7S-0.3GnP-700°C-1M HCl showed diamagnetism with a χ of -1.06×10^{-5} under 0.4 T at both 300 K and 150 K (Fig. 4d-e), indicating free from Fe^{2+}. When the temperature was decreased to 5 K, however, the 0.7S-0.3GnP-700°C-1M HCl showed ferromagnetic behavior with a saturation

magnetic moment reached 0.02 emu g^{-1} (Fig. 4f) due to the reduction in thermal fluctuation[46, 47], further supporting the intrinsic ferromagnetic properties in 0.7S-0.3GnP. This first experimentally confirmed intrinsic ferromagnetic properties in GnPs produced by ball-milling can be attributed to localized unpaired spins induced by the edge-doped sulfur heteroatoms. The presence of such unpaired electrons could increase the ionic conductivity in the 0.7S-0.3GnP to facilitate the lithium insertion/extraction during the discharge-charge process, and hence improve the S-GnP performance in LSBs.

To further test the effects of the S-doping-induced magnetic property and 'sandwich-like' meso-/macro-porous structure on the electrochemical performance of the 0.7S-0.3GnP cathode in LSBs, we prepared a reference sample by physically mixing 70 wt% sulfur with 30 wt% GnP (designated as: 70%S-30%GnP), in which the GnP was obtained through the same ball-milling procedure as for the S-GnP with only graphite as the starting material. We compared the electrochemical performance of 0.7S-0.3GnP with 70%S-30%GnP and GnP, respectively, after detecting no ferromagnetic behavior or 'sandwich-like' meso-porous structure for both 70%S-30%GnP and GnP. As shown in Fig. S7, the 0.7S-0.3GnP showed significantly higher capacity and rate capability than both the 70%S-30%GnP and GnP, indicating, once again, the important contributions of the 'spin effect' and 'sandwich-like' meso-porous structure induced by the edge-doping with S to improve electrochemical performance of the 0.7S-0.3GnP sample.

In conclusion, we have developed a simple one-step ball-milling method for low-cost and eco-friendly mass production of S-GnPs as efficient cathode materials (especially, 0.7S-0.3GnP) in lithium-sulfur batteries (LSBs). The 0.7S-0.3GnP cathode was demonstrated to deliver an initial reversible charge capacity of 1265.3 mAh g^{-1} at 0.1 C in the voltage range of 1.5 - 3.0 V with a high reversible capacity of 966.1 mAh g^{-1} at 2 C, a low capacity decay rate of 0.099% per cycle over 500 cycles, an excellent rate capability; attributable to the 'spin effect' and 'sandwich-like' mesoporous structure induced by the edge-doping with S. These results clearly indicate that the newly-developed S-GnP composites outperformed the current state-of-the-art cathode materials for LSBs and have a great potential for next generation high energy LIBs. Furthermore, the S-edge-doping-induced 'spin effect' and 'sandwich-like' mesoporous structure formation can be applied for the development of high-performance electrode materials for applications in other energy-related devices (*e.g.*, fuel cells, metal-air batteries, dye-sensitized solar cells) and chemical-/bio-sensors of practical significance.

Methods

Synthesis of S-graphene nanoplatelet (GnP) composites. To start with, stoichiometric amounts of commercial graphite and sulfur were placed into a stainless steel jar containing stainless steel balls (500 g, diameter 5 mm). Then, the jar was sealed and charged with argon after several charging–discharging cycles. Thereafter, the jar was fixed in a planetary ball-mill machine (TCI, USA) and agitated at 500 rpm for 48 h. Finally, the resultant powders were obtained and denoted as *x*S-*y*GnP (here, *x* and *y* represent the weight percentage of S and graphite, respectively, in the starting material; for example, 0.7S-0.3GnP stands for ball-milling with 70 wt% sulfur and 30 wt% graphite in the starting materials). The *x*S-*y*GnP samples were further heated at 700 °C with a temperature ramp of 2 ^{o}C min^{-1} in a tube furnace for 2 h under an argon flow (1000 s.c.c.m.) to remove physically adsorbed sulfur to produce the sample denoted as *x*S-*y*GnP-700°C. To get rid of any metallic impurities possibly from the ball-milling reactor and steel balls, the *x*S-*y*GnP-700°C samples were further purified by washing with 1M HCl to obtain *x*S-*y*GnP-700^{o}C-1M HCl samples. Meanwhile, a GnP sample was prepared by the same ball-milling procedure as those for the S-GnP samples, but without sulfur being introduced into the starting material.

Characterization. The phase identification of S-GnP compounds was carried out by powder X-ray diffraction (XRD, GBC MMA 017). The morphology of S-GnP was characterized by scanning electron microscopy (SEM) and transmission electron microscopy (TEM), using JSM-7500FA and JEOL JEM-2011 instruments, respectively. The elemental mapping of 0.7S-0.3GnP and 0.7S-0.3GnP-700^{o}C-1M HCl were carried out by energy dispersive X- ray spectroscopy (EDS) using the JSM-7500FA. The sulfur content of the S-GnP composites was determined by thermogravimetric analysis (TGA, TA Instruments 2000) under argon over a temperature range of 25 – 900 °C with a temperature ramp of 10 °C min^{-1}. The specific surface area was measured using 15 point N_2 absorption Brunauer-Emmett-Teller (BET) method using Quanta Chrome Nova 1000. X-ray photoelectron spectroscopy (XPS) measurements were carried out on a VG Scientific ESCALAB 2201XL instrument using aluminium Kα X-ray radiation. Raman spectra were collected using a Raman spectrometer (Lab RAM HR, Horiba Jobin Yvon SAS).

Electrochemical measurements. The electrochemical characterization of the S-GnP composites was carried out using coin cells. The electrodes were fabricated by blending the active material S-

GnP or 30%S-70%GnP (mixture of 30 wt% sulfur and 70 wt% GnP) powders with acetylene black and polyvinylidene fluoride (PVDF) binder in a weight ratio of 8 : 1 : 1. N-methyl-2-pyrrolidone (NMP) was used as the blending solvent for the mixture. The slurries were prepared using a Kurabo MAZERUSTAR planetary mixer, model KK-250S, for 15 min. The obtained slurry was coated on an Al foil, dried at 50 °C for 48 h, and then pressed under moderate pressure. 2032 coin-type cells were assembled in an Ar-filled glove box by stacking the as-prepared electrode as the working electrode, with Li foil as the counter electrode and reference electrode, a porous polypropylene film as separator, and 1 M lithium bis(trifluoromethanesulfonyl)imide in 1,3-dioxolane (DOL)/dimethoxyethane (DME) (1 : 1, v/v), including 0.1M $LiNO_3$, as the electrolyte. The cells were galvanostatically discharged and charged using an automatic battery testing system (Land®, China) at various current densities in a voltage range of 1.5 - 3.0 V at room temperature. Electrochemical impedance spectroscopy (EIS) and cyclic voltammetry (CV) measurements were performed on a Biologic MVP 3 electrochemical workstation. Electrochemical impedance spectroscopy (EIS) measurements were performed over the frequency range of 10 mHz to 1 M Hz. Cyclic voltammogram measurements were performed at a scan rate of 0.1 mV s^{-1} in a voltage range of 1.5 - 3.0 V.

References

1. Goodenough JB, Kim Y. Challenges for rechargeable Li batteries. *Chem. Mater.* **22**, 587-603 (2009).
2. Etacheri V, Marom R, Elazari R, Salitra G, Aurbach D. Challenges in the development of advanced Li-ion batteries: a review. *Energ. Environ. Sci.* **4**, 3243-3262 (2011).
3. Xu JT, Dou SX, Liu HK, Dai LM. Cathode materials for next generation lithium ion batteries. *Nano Energy* **2**, 439-442 (2013).
4. Evers S, Nazar LF. New approaches for high energy density lithium–sulfur battery cathodes. *Acc. Chem. Res.* **46**, 1135-1143 (2012).
5. Manthiram A, Fu Y, Su Y-S. Challenges and prospects of lithium–sulfur batteries. *Acc. Chem. Res.* **46**, 1125-1134 (2012).
6. Wang J*, et al.* Sulfur–mesoporous carbon composites in conjunction with a novel ionic liquid electrolyte for lithium rechargeable batteries. *Carbon* **46**, 229-235 (2008).
7. Ji X, Lee KT, Nazar LF. A highly ordered nanostructured carbon–sulphur cathode for lithium–sulphur batteries. *Nat. Mater.* **8**, 500-506 (2009).
8. Ji X, Evers S, Black R, Nazar LF. Stabilizing lithium-sulphur cathodes using polysulphide reservoirs. *Nat. Commun.* **2**, 1293 (2011).
9. Jayaprakash N, Shen J, Moganty SS, Corona A, Archer LA. Porous hollow carbon@sulfur composites for high-power lithium-sulfur batteries. *Angew. Chem. Int. Ed.* **50**, 5904-5908 (2011).

10. Schuster J*, et al.* Spherical ordered mesoporous carbon nanoparticles with high porosity for lithium-sulfur batteries. *Angew. Chem. Int. Ed.* **51**, 3591-3595 (2012).
11. Huang C*, et al.* Manipulating surface reactions in lithium-sulphur batteries using hybrid anode structures. *Nat. Commun.* **5**, 4343 (2014).
12. Zhang B, Qin X, Li G, Gao X. Enhancement of long stability of sulfur cathode by encapsulating sulfur into micropores of carbon spheres. *Energ. Environ. Sci.* **3**, 1531-1537 (2010).
13. Zheng G, Yang Y, Cha JJ, Hong SS, Cui Y. Hollow carbon nanofiber-encapsulated sulfur cathodes for high specific capacity rechargeable lithium batteries. *Nano Lett.* **11**, 4462-4467 (2011).
14. Zhang CF, Wu HB, Yuan CZ, Guo ZP, Lou XW. Confining sulfur in double-shelled hollow carbon spheres for lithium-sulfur batteries. *Angew. Chem. Int. Ed.* **51**, 9592-9595 (2012).
15. Yuan L, Yuan H, Qiu X, Chen L, Zhu W. Improvement of cycle property of sulfur-coated multi-walled carbon nanotubes composite cathode for lithium/sulfur batteries. *J. Power Sources* **189**, 1141-1146 (2009).
16. Guo J, Xu Y, Wang C. Sulfur-impregnated disordered carbon nanotubes cathode for lithium–sulfur batteries. *Nano Lett.* **11**, 4288-4294 (2011).
17. Elazari R, Salitra G, Garsuch A, Panchenko A, Aurbach D. Sulfur-impregnated activated carbon fiber cloth as a binder-free cathode for rechargeable Li-S batteries. *Adv. Mater.* **23**, 5641-5644 (2011).
18. Zhao M-Q*, et al.* Graphene/single-walled carbon nanotube hybrids: one-step catalytic growth and applications for high-rate Li–S batteries. *ACS Nano* **6**, 10759-10769 (2012).
19. Lu S, Cheng Y, Wu X, Liu J. Significantly improved long-cycle stability in high-rate Li–S batteries enabled by coaxial graphene wrapping over sulfur-coated carbon nanofibers. *Nano Lett.* **13**, 2485-2489 (2013).
20. Wang H*, et al.* Graphene-wrapped sulfur particles as a rechargeable lithium–sulfur battery cathode material with high capacity and cycling stability. *Nano Lett.* **11**, 2644-2647 (2011).
21. Ji L*, et al.* Graphene oxide as a sulfur immobilizer in high performance lithium/sulfur cells. *J. Am. Chem. Soc.* **133**, 18522-18525 (2011).
22. Sun H*, et al.* A composite material of uniformly dispersed sulfur on reduced graphene oxide: Aqueous one-pot synthesis, characterization and excellent performance as the cathode in rechargeable lithium-sulfur batteries. *Nano Res.* **5**, 726-738 (2012).
23. Zhou G*, et al.* Fibrous hybrid of graphene and sulfur nanocrystals for high-performance lithium–sulfur batteries. *ACS Nano* **7**, 5367-5375 (2013).
24. Lin T*, et al.* Scotch-tape-like exfoliation of graphite assisted with elemental sulfur and graphene-sulfur composites for high-performance lithium-sulfur batteries. *Energ. Environ. Sci.* **6**, 1283-1290 (2013).
25. Lu S, Chen Y, Wu X, Wang Z, Li Y. Three-dimensional sulfur/graphene multifunctional hybrid sponges for lithium-sulfur batteries with large areal mass loading. *Sci Rep-Uk* **4**, (2014).
26. Rong J, Ge M, Fang X, Zhou C. Solution ionic strength engineering ss a generic strategy to coat graphene oxide (GO) on various functional particles and its application in high-performance lithium–sulfur (Li–S) batteries. *Nano Lett*. **14**, 473-479 (2013).
27. Chen R*, et al.* Graphene-Based three-dimensional hierarchical sandwich-type architecture for high-performance Li/S batteries. *Nano Lett.* **13**, 4642-4649 (2013).

28. Zhao M-Q*, et al.* Unstacked double-layer templated graphene for high-rate lithium–sulphur batteries. *Nat Commun.* **5**, 3410 (2014).
29. Zhou G*, et al.* A Graphene–pure-sulfur sandwich structure for ultrafast, long-life lithium–sulfur batteries. *Adv. Mater.* **26**, 625-631 (2014).
30. Song M-K, Zhang Y, Cairns EJ. A Long-Life, High-rate lithium/sulfur cell: A multifaceted approach to enhancing cell performance. *Nano Lett.* **13**, 5891-5899 (2013).
31. Zhou G*, et al.* A flexible nanostructured sulphur–carbon nanotube cathode with high rate performance for Li-S batteries. *Energ. Environ. Sci.* **5**, 8901-8906 (2012).
32. Wang J, Yang J, Xie J, Xu N. A novel conductive polymer–sulfur composite cathode material for rechargeable lithium batteries. *Adv. Mater.* **14**, 963-965 (2002).
33. Yang Y*, et al.* Improving the performance of lithium–sulfur batteries by conductive polymer coating. *ACS Nano* **5**, 9187-9193 (2011).
34. Xiao L*, et al.* A Soft Approach to encapsulate sulfur: polyaniline nanotubes for lithium-sulfur batteries with long cycle life. *Adv. Mater.* **24**, 1176-1181 (2012).
35. Li W, Zheng G, Yang Y, Seh ZW, Liu N, Cui Y. High-performance hollow sulfur nanostructured battery cathode through a scalable, room temperature, one-step, bottom-up approach. *Proc. Natl. Acad. Sci.* **110**, 7148-7153 (2013).
36. Wang L, Dong Z, Wang D, Zhang F, Jin J. Covalent bond glued sulfur nanosheet-based cathode integration for long-cycle-life Li–S batteries. *Nano Lett.* **13**, 6244-6250 (2013).
37. Li W, Zhang Q, Zheng G, Seh ZW, Yao H, Cui Y. Understanding the role of different conductive polymers in improving the nanostructured sulfur cathode performance. *Nano Lett.* **13**, 5534-5540 (2013).
38. Hummers Jr WS, Offeman RE. Preparation of graphitic oxide. *J. Am. Chem. Soc.* **80**, 1339-1339 (1958).
39. Jeon IY*, et al.* Edge-carboxylated graphene nanosheets via ball milling. *Proc. Natl. Acad. Sci. USA* **109**, 5588-5593 (2012).
40. Jeon IY*, et al.* Facile, scalable synthesis of edge-halogenated graphene nanoplatelets as efficient metal-free eletrocatalysts for oxygen reduction reaction. *Sci Rep-Uk* **3**, (2013).
41. Jeon IY*, et al.* Large-Scale Production of edge-Selectively functionalized graphene nanoplatelets via ball milling and their use as metal-free electrocatalysts for oxygen reduction reaction. *J. Am. Chem. Soc.* **135**, 1386-1393 (2013).
42. Jeon IY*, et al.* Edge-Selectively sulfurized graphene nanoplatelets as efficient metal-free electrocatalysts for oxygen reduction reaction: The electron Spin effect. *Adv. Mater.* **25**, 6138-6145 (2013).
43. Deng D*, et al.* Toward N-doped graphene via solvothermal synthesis. *Chem. Mater.* **23**, 1188-1193 (2011).
44. Choi E-K, Jeon I-Y, Oh S-J, Baek J-B. "Direct" grafting of linear macromolecular "wedges" to the edge of pristine graphite to prepare edge-functionalized graphene-based polymer composites. *J. Mater. Chem.* **20**, 10936-10942 (2010).
45. Xu JT, Chou SL, Gu QF, Liu HK, Dou SX. The effect of different binders on electrochemical properties of $LiNi_{1/3}Mn_{1/3}C_{1/3}O_2$ cathode material in lithium ion batteries. *J. Power Sources* **225**, 172-178 (2013).
46. Nair R*, et al.* Spin-half paramagnetism in graphene induced by point defects. *Nat. Phys.* **8**, 199-202 (2012).
47. Nair RR*, et al.* Dual origin of defect magnetism in graphene and its reversible switching by molecular doping. *Nat. Commun.* **4**, 3010 (2013).

Acknowledgments

The authors are grateful for financial support from the Auto CRC 2020, the Air Force Office of Scientific Research (AFOSR) (FA9550-12-1-0037, FA-9550-12-1-0069), and the National Science Foundation (NSF) (NSF-AIR-IIP-1343270, NSF-DMR-1106160).The authors thank Dr. T. Silver for critical reading of the manuscript.

Author contributions

J. Xu and L. Dai conceived and designed the experiments. J. Xu, J. Shui and M. Wang synthesized the materials and performed the materials characterizations and electrochemical measurements. J. Xu, J. Wang and S. Dou carried out the magnetic measurements. I. Jeon, J. Seo and J. Baek conducted the materials preparation and results discussion. S. Dou, H. Liu and L. Dai were responsible for planning and supervising the project. J. Xu, S. Dou, J. Baek and L. Dai co-wrote the paper and all authors discussed the results and commented on the manuscript.

Additional information

Supplementary Information accompanies this paper on
http://www.nature.com/naturecommunications

Competing financial interests: The authors declare no competing financial interests.

Figures

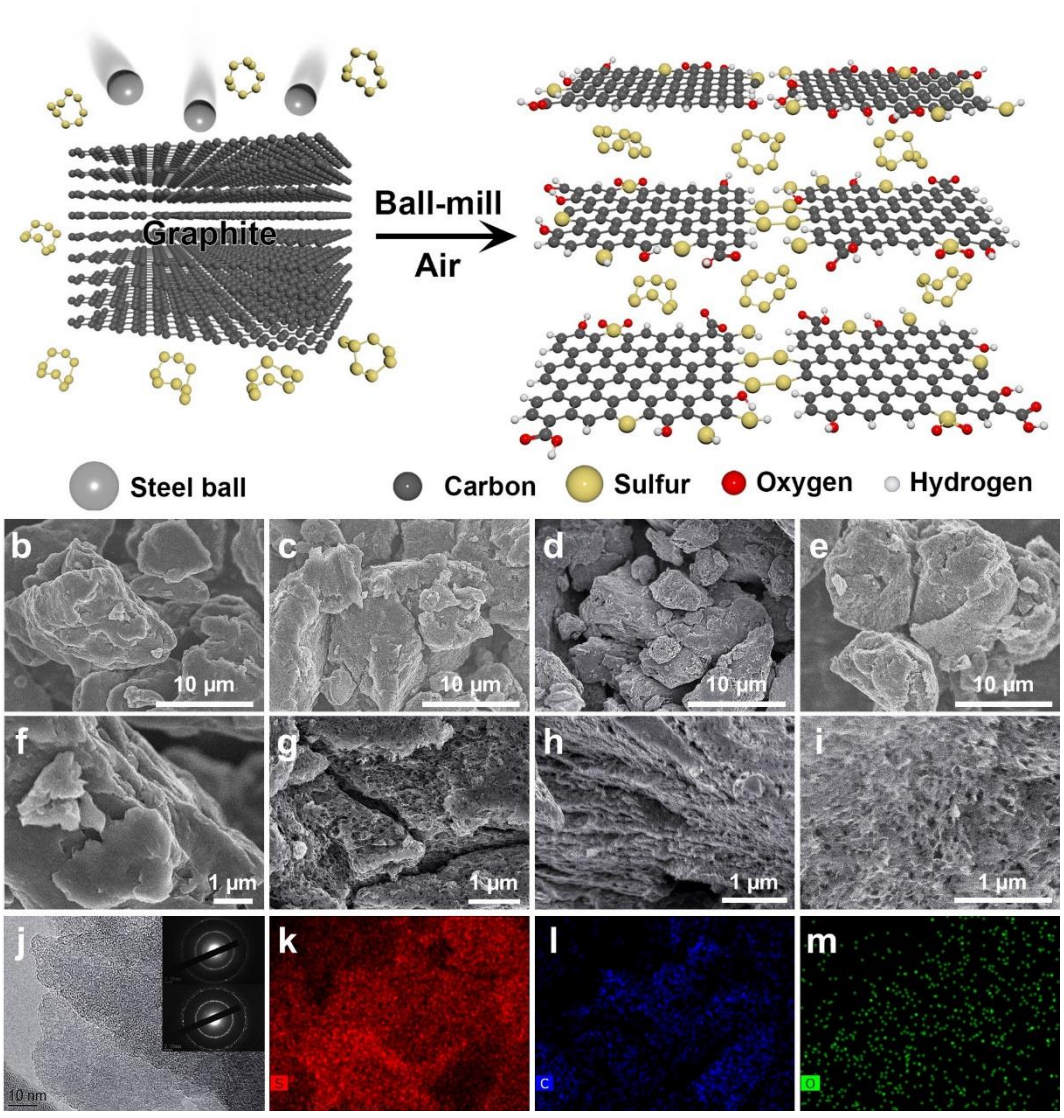

Figure 1. Preparation of S-GnPs by ball milling and microscopic characterization. (a) Schematic representation of the S-GnP preparation; and SEM images at different magnifications for samples with different starting compositions: (b, f) 0.5S-0.5GnP; (c, g) 0.6S-0.4GnP; (d, h) 0.7S-0.3GnP; and (e, i) 0.8S-0.2GnP. (j) TEM image of 0.7S-0.3GnP, with the insets showing the corresponding SAED patterns from the edge (*top*) and basal plane (*bottom*), respectively; SEM elemental mappings for 0.7S-0.3GnP: (k) sulfur, (l) carbon and (m) oxygen by energy dispersive X-ray spectroscopy (EDS).

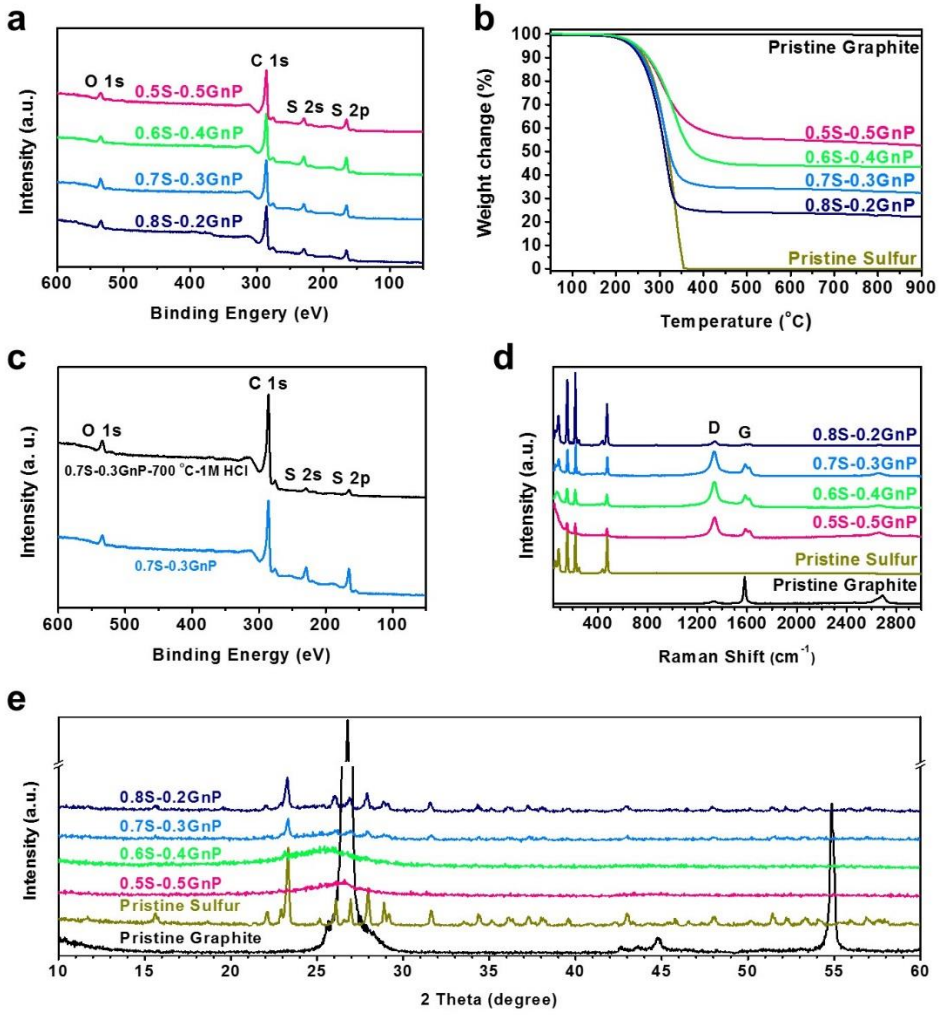

Figure 2. Spectroscopic characterization of S-GnPs. (a) X-ray photoelectron spectroscopy (XPS) for the S-GnPs; (b) thermogravimetric analysis (TGA) for the S-GnPs, graphite and sulfur; (c) XPS for the 0.7S-0.3GnP and 0.7S-0.3GnP-700°C-1M HCl (see text); (d) Raman spectroscopy for the S-GnPs, graphite, and sulfur; and (e) X-ray diffraction (XRD) patterns for the S-GnPs, graphite, and sulfur.

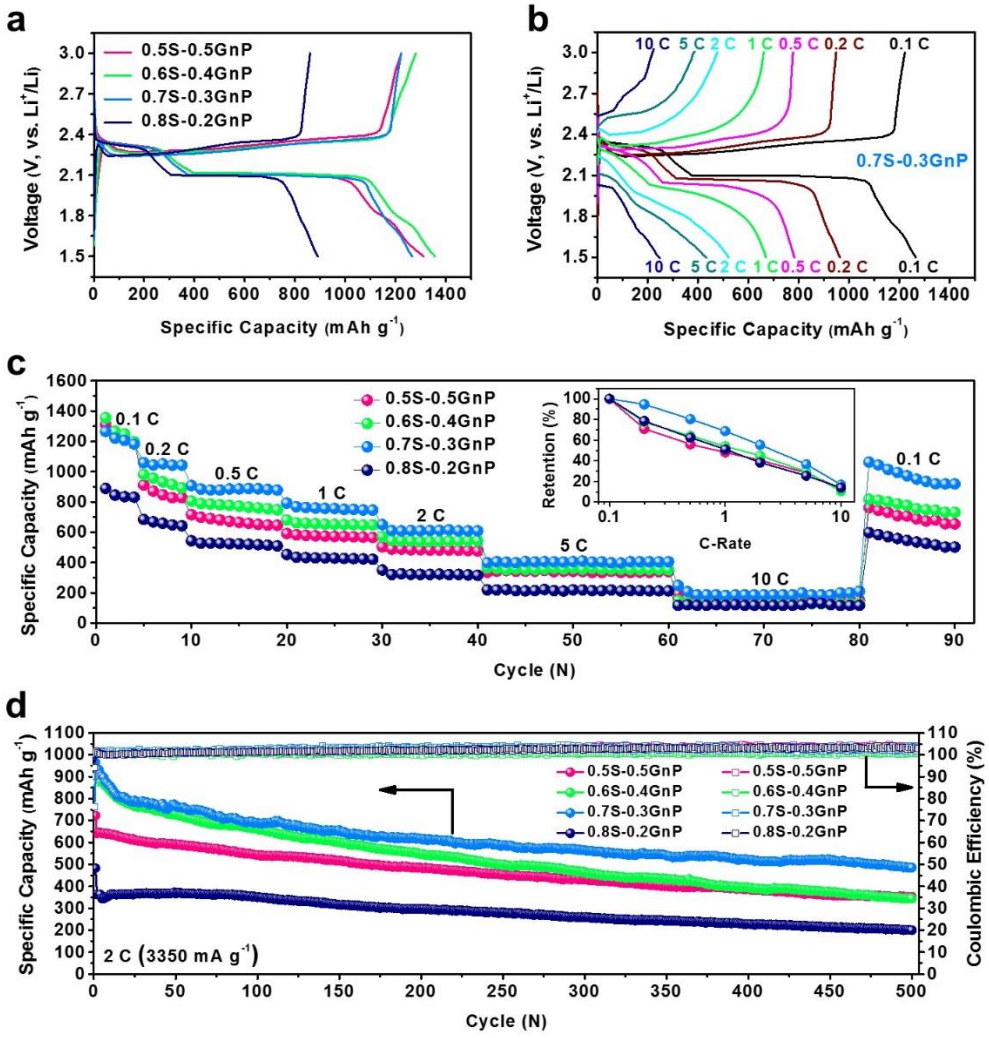

Figure 3. Evaluation of S-GnP cathodes for LSBs. (a) Discharge-charge profiles of S-GnPs at 0.1 C; (b) discharge-charge profiles for 0.7S-0.3GnP at various C-rates; (c) rate capabilities of S-GnPs, with the inset showing the percentage capacity retention as a function of the C-rate; and (d) cycling performance of S-GnPs at 2 C (3350 mAh g^{-1}) in the voltage range of 1.5 - 3.0 V.

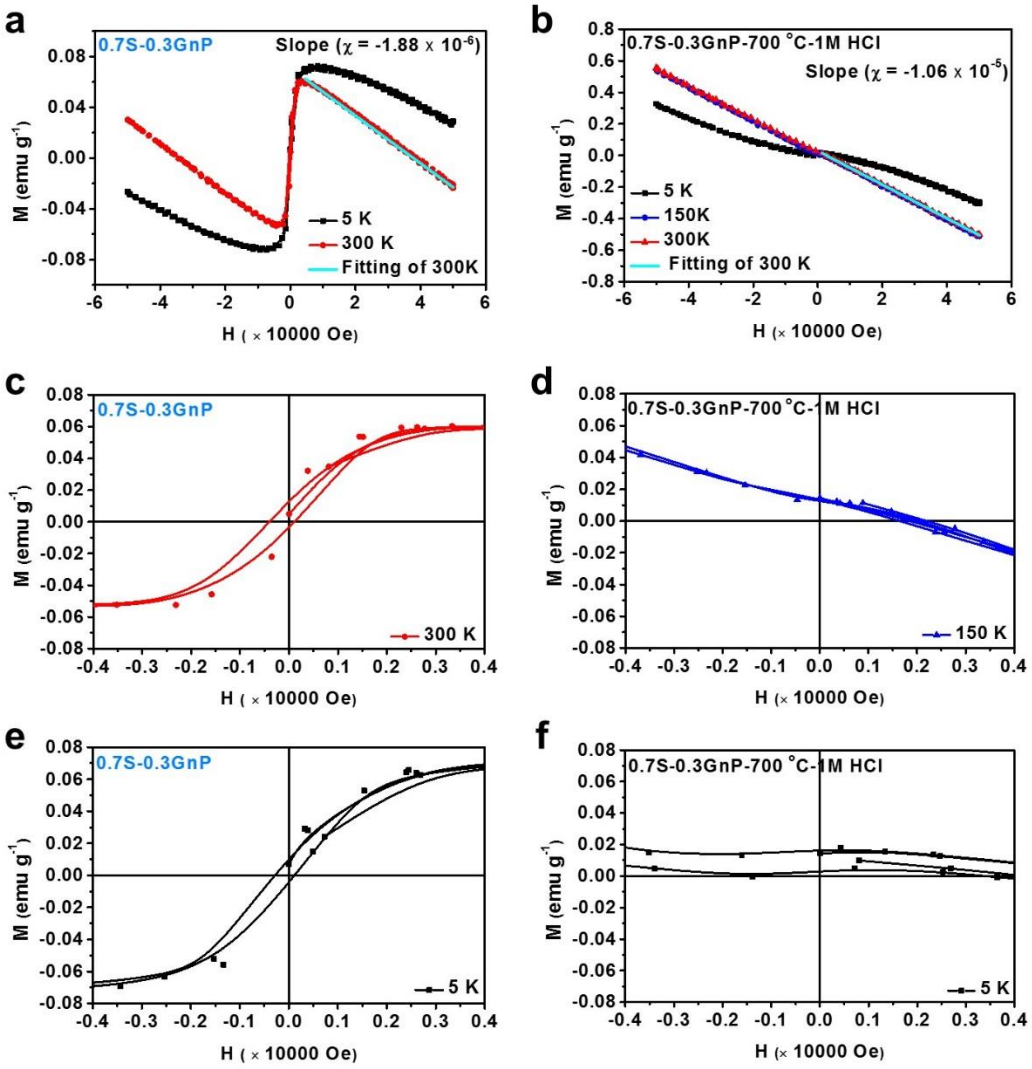

Figure 4. Ferromagnetic property of GnPs and its effects on their cathodic performance. Temperature-dependent magnetization curves for (a) 0.7S-0.3GnP at 5 K and 300 K, magnifications of (a) at 300 K(b) and 5 K(c); and (d) 0.7S-0.3GnP-700ºC-1M HCl at 5 K, 150 K, and 300 K, magnifications of (d) at 150 K(e) and 5 K(f).